Research Square

Preprints are preliminary reports that have not undergone peer review.
They should not be considered conclusive, used to inform clinical practice,
or referenced by the media as validated information.

An XPBD Adhesive-Bond Simulation Model toward Qualitative Reproduction of Sticky-Food Release Behavior

Ryota Adachi

22hs251a@shinshu-u.ac.jp

Shinshu University

Kimitoshi Yamazaki

Tohoku University

Jun-ya Takayama

Shinshu University

Research Article

Keywords: robotic food handling, sticky-food release, extended position-based dynamics, adhesive bonds, residual adhesion

Posted Date: November 24th, 2026

DOI: https://doi.org/10.21203/rs.3.rs-11320682/v1

License: This work is licensed under a Creative Commons Attribution 4.0 International License.
Read Full License

Additional Declarations: No competing interests reported.

An XPBD Adhesive-Bond Simulation Model toward Qualitative Reproduction of Sticky-Food Release Behavior

Ryota Adachi[1], Kimitoshi Yamazaki[2], Jun-ya Takayama[3]

[1] Department of Science and Technology, Graduate School of Medicine, Science and Technology, Shinshu University, Nagano, Japan; [2] Department of Robotics, Graduate School of Engineering, Tohoku University, Miyagi, Japan; [3] Department of Mechanical Systems Engineering, Faculty of Engineering, Shinshu University, Nagano, Japan.

※Corresponding author: Ryota Adachi, email: 22hs251a@shinshu-u.ac.jp

This study presents a two-dimensional simulation model for examining sticky-food release. The model combines a deformable body based on Extended Position-Based Dynamics (XPBD) with adhesive bonds whose rupture is governed by the maximum effective-opening history. Release behavior was examined with and without support from the placement surface at the onset of gripper opening. The simulations showed lateral drag as the food followed the finger to which it remained attached. Lateral displacement was smaller when the food was supported by the placement surface during opening. Experiments with Japanese rice cake showed similar qualitative trends.

Keywords: robotic food handling; sticky-food release; extended position-based dynamics; adhesive bonds; residual adhesion

1. Introduction

Automating food handling with robots is challenging because food items vary in shape, deformability, and surface characteristics [1]. For soft and adhesive foods, release is a particular difficulty: an item can remain attached to the fingers during gripper opening and move away from its intended placement position.

We refer to attachment that persists after gripper opening begins as residual adhesion. When the food detaches from one finger while remaining attached to the other, it can follow the retracting finger and move laterally; we call this motion lateral drag. This study examines which finger retains the food during prescribed gripper opening and how contact with the placement surface relates to lateral motion and detachment. To investigate these questions, we develop a computational model that tracks adhesive-bond formation, persistence, and history-dependent rupture, and compare simulated and experimental motion patterns qualitatively.

The primary contributions of this paper are the following two points.

- We develop a two-dimensional model based on Extended Position-Based Dynamics (XPBD) with history-dependent adhesive-bond rupture to examine the relationship between residual adhesion and lateral food motion during gripper opening.
- We measure final lateral displacement in release experiments using Japanese rice cake with and without initial support from the placement surface, and compare the observed and simulated motion patterns qualitatively.

The remainder of this paper is organized as follows: Section 2 reviews related work. Section 3 details the proposed computational model. Sections 4 and 5 report the simulation results and physical experiments, respectively. Section 6 compares their motion patterns and discusses the limitations of the current approach, while Section 7 concludes the paper.

2. Related Work

2.1 Food Handling, Release, and Placement

Wang et al. [1] review robotic food handling from three perspectives: end-effectors, food recognition, and basic information about food relevant to handling, including physical properties and classification. Qiu et al. [2] propose an evaluation system to support the selection and design of food-handling end-effectors. Their assessment of adaptability to sticky foods uses positional error after placement, highlighting the relevance of adhesion to placement performance.

Ueda et al. [3] examine how vibration amplitude, frequency, rod inclination, and vibration direction affect the slipping and detachment of pork slices adhering to a metal rod representing a gripper finger. For placement tasks, it is important to consider both detachment from the gripper and food motion during release.

2.2 Simulation of Deformable Bodies and Adhesive Contact

Position-Based Dynamics (PBD) corrects particle positions to satisfy constraints [4] and has been extended to simulate continuum materials [5]. Extended Position-Based Dynamics (XPBD) introduces compliance to reduce the dependence of simulated stiffness on the time step and the number of solver iterations [6].

Models and numerical methods have also been proposed for adhesive contact involving deformable bodies. Gascón et al. [7] add adhesive constraints to a constraint-based contact solver that uses projected Gauss–Seidel iterations. The adhesion strength at each contact evolves according to bonding and debonding laws. Fang et al. [8] incorporate distance-dependent normal adhesion and a semi-implicit treatment of tangential adhesion into Incremental Potential Contact (IPC). Their examples of plate separation and tape peeling illustrate how detachment depends on the load distribution and peeling direction. These methods have also been demonstrated in simulated food scenes, including candy [7] and sushi [8].

Models of adhesion and detachment have also been used to generate robot motions. For food handling, Suzuki and Mizuuchi [9] simulate adhesion between rigid cubes and use reinforcement learning to learn separation motions. In a medical application, AutoPeel [10] optimizes robotic peeling trajectories using a differentiable simulation of adhesion and peeling. Its model connects the skin and a wound dressing by zero-rest-length spring constraints in XPBD and releases a constraint, by setting its stiffness to zero, once the spring's potential energy reaches a threshold.

The experimental food-handling studies [2,3] provide evidence for evaluating end-effectors and methods for facilitating detachment. To inform the design of release motions for accurate placement, it is important to examine how adhesion persisting during release relates to the motion that leads to the final placement position. The modeling approaches reviewed above provide computational tools for investigating this relationship, while the applications in [9,10] illustrate how adhesion models can support motion generation. The present study therefore develops a two-dimensional simulation model to examine how residual adhesion and detachment relate to lateral food motion during prescribed gripper opening. XPBD [6] is used so that food deformation and adhesive-bond constraints can be handled within a single position-correction loop (Section 3).

3. Proposed Simulation Model

3.1 Problem Setting and Overview of the Proposed Method

The proposed model consists of the following three components, which are solved in a single position-based time-integration loop (Fig. 1).

- A two-dimensional deformable body represented by vertices and a triangular mesh (elastic, viscoelastic, and plastic; Section 3.2.1) [5]
- An adhesive-bond model based on the maximum effective-opening history and internal opening work (Section 3.2.2)

- Non-penetration, restitution, and friction at rigid gripper fingers and the placement surface, referred to below as the floor (Section 3.2.3)

The model represents a two-dimensional cross-section of the food to examine sideways motion, stretching, and compression during release. Each gripper finger is a rigid line segment that follows a prescribed trajectory. Forces from the food do not change the finger motion. These simplifications reduce the degrees of freedom and allow the effect of adhesion to be studied under the same opening motion. Deformation is computed using position-based material and XPBD formulations [5,6] with substepping [11]. Bond formation, rupture, and renewed attachment are handled in the same integration loop. Motion outside the cross-section is not represented.

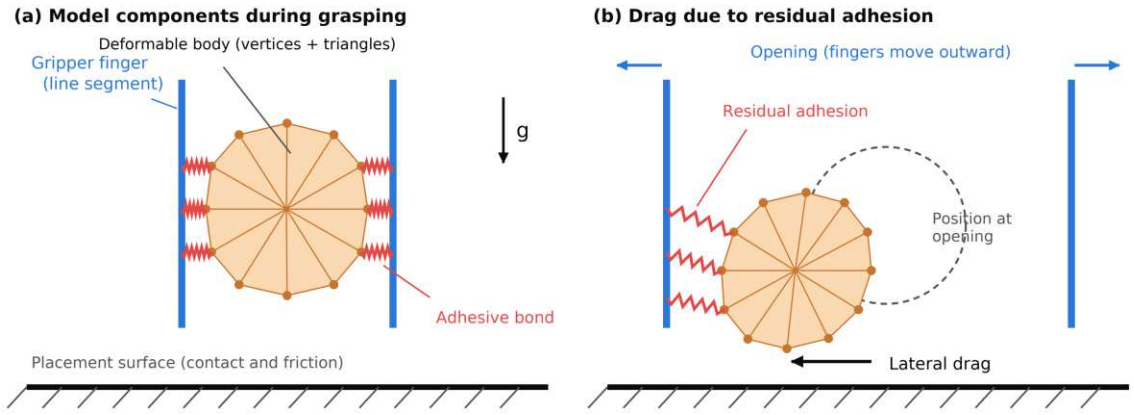

Fig. 1 Structure of the proposed model. (a) Deformable body, adhesive bonds, gripper fingers approximated as line segments, and placement surface. (b) Adhesive bonds that remain during opening (residual adhesion) pull the food toward one finger (lateral drag).

3.2 Model

3.2.1 Deformation Model

The deformation of the model gives the Green–Lagrange strain, and a St. Venant–Kirchhoff energy describes elastic deformation [12]. Plastic and viscous strains shift the strain entering this energy. Plastic

strain evolves when the norm of the deviatoric elastic strain exceeds the yield parameter. A standard linear solid (SLS) represents stress relaxation: its viscous strain relaxes toward the elastic strain, and the relaxation-branch fraction specifies the fraction of instantaneous stiffness that relaxes. For each element, XPBD solves a constraint equal to the square root of its elastic energy [5,6]. An area-barrier constraint limits compression of the signed triangle area, but later corrections can still cause collapse or inversion.

3.2.2 Adhesion and Detachment Model

A bond connects a food surface vertex i to an anchor p. At formation, $p = q + (R + t_s)n$, where q is the closest point on the rigid segment, n its normal, R the contact radius, and t_s the adhesive-layer thickness (Fig. 2(a)). The anchor's position relative to the segment remains fixed. A vertex without an active bond can bond to an enabled adhesive face when $d - R \leq t_s$, where d is its distance to the segment. Thus, the 1 mm adhesive layer can capture vertices before hard floor contact at a clearance of 10^{-9} m or less.

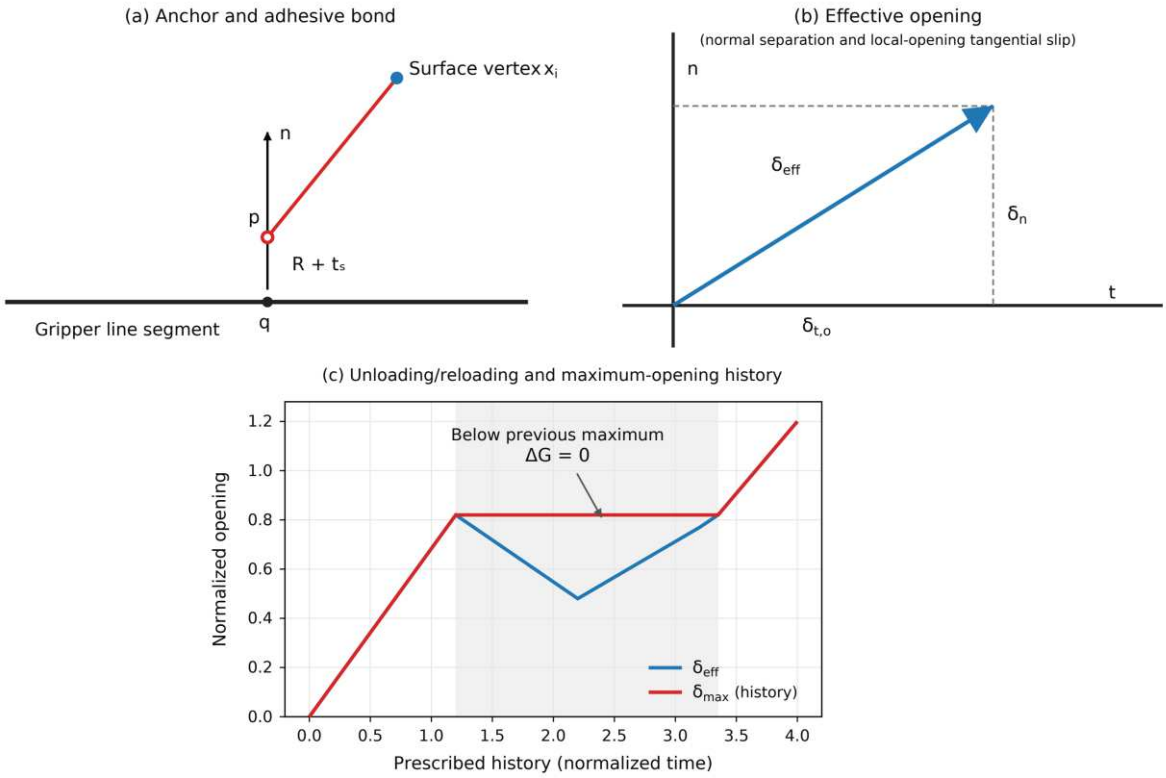

121

122 **Fig. 2 Adhesive-bond model. (a) Anchor geometry; (b) effective opening from normal separation and tangential**
123 **slip; (c) unloading, reloading, and maximum-opening history.**

124 **Effective opening and maximum history**

125 The normal and tangential separations from the anchor are

$$\delta_{\mathrm{n}} = n \cdot (x_{\mathrm{i}} - p), \qquad \delta_{\mathrm{t}} = t \cdot (x_{\mathrm{i}} - p), \tag{1}$$

126 where t is the unit tangent. Rupture uses an effective tangential separation $\delta_{\mathrm{t,o}}$ that distinguishes slip
127 during local closure from slip during local opening. The subscript o denotes this opening-dependent
128 measure; it does not refer to the time of the gripper command.

129 Define

$$g = \min\left(1, \max\left(0, \frac{\max(0, \delta_{\mathrm{n}}) - \varepsilon}{\varepsilon}\right)\right), \tag{2}$$

130 with $\varepsilon = \max(10^{-9}\ \mathrm{m}, 0.05R)$. The effective tangential separation is

$$\delta_{\mathrm{t,o}} = (1 - g)\max(|\delta_{\mathrm{t}}| - d_{\mathrm{t}}, 0) + g|\delta_{\mathrm{t}} - \delta_{\mathrm{t,ref}}|, \quad (3)$$

where $d_{\mathrm{t}} = 5$ mm is the slip tolerance during closure. The reference $\delta_{\mathrm{t,ref}}$ is updated to the current δ_{t} whenever $g = 0$. As normal separation increases from ε to 2ε, g rises from zero to one and shifts the measure toward slip from this stored reference.

Equation (4) combines normal and effective tangential separation (Fig. 2(b)). Eq. (5) stores its maximum, and Eq. (6) accumulates internal opening work only when that maximum increases. New bonds start with zero maximum-opening history and work. Unloading and reloading below the previous maximum add no work (Fig. 2(c)).

$$\delta_{\mathrm{eff}} = \sqrt{\max(0, \delta_n)^2 + \delta_{t,o}^2} \quad (4)$$

$$\delta_{\mathrm{max,k}} = \max\left(\delta_{\mathrm{max,k-1}}, \delta_{\mathrm{eff},k}\right) \quad (5)$$

$$G_k = G_{k-1} + K_G\, \delta_{\mathrm{eff},k} \left(\delta_{\mathrm{max,k}} - \delta_{\mathrm{max,k-1}}\right) \quad (6)$$

Damage and rupture

For continuous monotonic opening, the update in Eq. (6) gives the following work and reference rupture opening:

$$G = \frac{K_G \delta_{\mathrm{max}}{}^2}{2} \quad (7)$$

$$\delta_b = \sqrt{\frac{2G_c}{K_G}} \quad (8)$$

Equations (7) and (8) give reference scales (Table 1). The finite-substep update in Eq. (6) uses right-endpoint increments, so the reference opening is not an exact discrete rupture distance. G and G_{c} are internal bond-level work measures, not measured fracture energies. The coefficient K_{G} converts squared opening into this internal scale and is independent of the XPBD compliance. The normalized damage D_{E} is defined in Eq. (9), and the bond is removed when the condition in Eq. (10) is met. D_{E} is used to track proximity to rupture; it does not soften a surviving bond.

$$D_{E,k}=\min\left(\frac{G_k}{G_c},\,1\right) \tag{9}$$

$$G_k \geq G_c \tag{10}$$

A bond is also removed if its food vertex crosses to the back side of the finger segment, or if damage is within 10^{-6} of one while normal opening is positive. The evaluation also includes a control condition that removes finger bonds when the gripper starts opening (Section 4.1).

XPBD update of adhesive constraints

The normal and tangential anchor constraints are $C_{\mathrm{n}} = \max(0, \delta_{\mathrm{n}})$, $C_{\mathrm{t}} = \delta_{\mathrm{t}}$. The tangential constraint uses the displacement from the anchor, whereas the rupture history uses $\delta_{\mathrm{t,o}}$. The corresponding compliances c_{n} and c_{t} remain fixed until the bond is removed. Equation (11) gives the XPBD multiplier increment for a scalar constraint C [6]. The multiplier is reset at the start of each substep.

$$\Delta\lambda = \frac{-C(x) - \tilde{\alpha}\lambda}{\sum_i w_i \|\nabla_i C(x)\|^2 + \tilde{\alpha}} \tag{11}$$

Here, λ is the accumulated multiplier, α is the constraint compliance, and h is the substep width. The compliance scaled by the time step is

$$\tilde{\alpha} = \frac{\alpha}{h^2} \tag{12}$$

The corresponding position correction is

$$\Delta x_i = w_i \nabla_i C \, \Delta\lambda \tag{13}$$

where w_i is the inverse vertex mass. The normal and tangential constraints use $\alpha = c_{\mathrm{n}}$ and $\alpha = c_{\mathrm{t}}$, respectively. The rigid anchor has zero inverse mass.

After opening, new bonds can form under the same distance and surface-eligibility conditions. Each new bond starts with zero history. Whether finger bonds are retained or may form again depends on the condition in Section 4.1.

3.2.3 Contact and Friction Model

Non-penetration keeps each surface vertex at least a distance R from a rigid segment. Hard position projection enforces this condition. Before this projection, a continuous collision check compares the motion of each vertex with that of the segments within the substep; a vertex that would cross a segment is placed on the non-penetrating side of the segment at its end-of-substep position (Algorithm 1, line 12). Restitution and Coulomb friction are then applied as velocity impulses based on the relative motion of the vertex and the segment. These contact operations are performed in the same integration loop as the XPBD deformation and adhesion updates.

3.3 Numerical Method

Algorithm 1 summarizes one substep of the coupled deformation, adhesion, and contact update.

Algorithm 1 Simulation update for one substep

1: Update prescribed boundary motion and adhesion conditions (Section 4.1).
2: Predict positions and reset XPBD multipliers.
3: Solve food-deformation constraints, including the area barrier.
4: for each active adhesive bond do
5: Update $\delta_{\mathrm{eff},k}$, $\delta_{\mathrm{max,k}}$, G_k, and $D_{E,k}$ using Eqs. (1)–(6) and (9).
6: **if** $G_k \geq G_c$ [Eq. (10)] or another removal condition holds **then**
7: Remove the bond.
8: else
9: Solve C_{n} and C_{t} by XPBD with fixed c_{n} and c_{t} [Eqs. (11)–(13)].
10: end if
11: end for
12: Resolve collisions and contact, including area-barrier corrections.

13: Update material histories and velocities; apply damping and contact impulses.

14: Form eligible new bonds; set $\delta_{\max} \leftarrow 0$, $G \leftarrow 0$, and $D_{\mathrm{E}} \leftarrow 0$.

Other removal conditions are given in Section 3.2.2. For a back-side crossing, the bond is removed without updating its opening history or work.

4. Simulation Results

To evaluate the proposed XPBD-based adhesion model, we conducted simulations to examine how residual adhesion and physical support affect the release motion of sticky foods. The simulations employed two main procedures: drop release, where the gripper opens above the floor, and grounded release, where it opens with the food in contact with the floor.

This section is organized to systematically present the qualitative verification of the model. Section 4.1 details the evaluation conditions, including the object shapes and adhesion settings. Section 4.2 analyzes the post-opening motion under retained, removed, and increased finger adhesion. Section 4.3 investigates the relation between lateral motion and the side of the remaining bonds. Finally, Section 4.4 examines bond evolution and lateral displacement under the grounded-release procedure.

It is important to note that these simulations examine behavior using a simplified two-dimensional model, and the material and interface parameters have not been calibrated to the experimental specimens. Furthermore, element inversion—where a triangle's signed area becomes nonpositive—occurred in every tested condition. Such a state does not represent a physically admissible deformation of the food. Although calculations continued after these events to inspect the model's numerical behavior, the effect on subsequent motion remains unknown. Therefore, the following results serve to explore qualitative motion patterns rather than to establish quantitative predictive accuracy.

4.1 Evaluation Conditions

Three food shapes were used (Fig. 3). S0 has a left–right symmetric initial outline. S+ has a flat face that contacts the finger on the right side, and S- is the mirror image of S+. S+ and S- are intended to leave adhesion on the finger on the flat-face side.

Three finger-adhesion conditions were compared. The first retains finger bonds after opening, allows new bonds on renewed contact, and uses the rupture rule in Section 3.2.2. This condition is called ON. The second removes all finger bonds at opening and prevents new ones from forming; it is called OFF. The third uses the same rules as ON but increases the finger-bond rupture threshold fivefold; it is called HIGH. The floor uses the same bond law and constants as the fingers in ON, including when the finger condition is HIGH. Floor adhesion is enabled at the start of the opening stage, before the fingers move apart. Non-penetration and friction remain active throughout.

Each condition is denoted as shape·adhesion. Drop release comprised S0·ON, S+·ON, S-·ON, S+·OFF, S-·OFF, and S+·HIGH. Grounded release comprised S+·ON and S+·HIGH. The release procedure is identified separately in the text and figures.

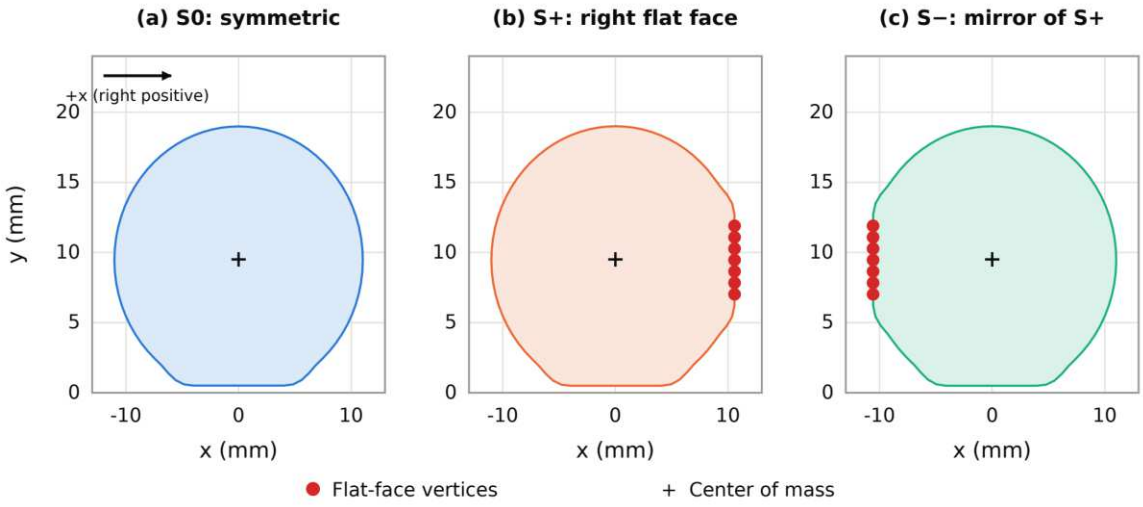

Fig. 3 Three shapes used in the evaluation. Red dots are the boundary vertices of the flat face contacting the finger in S±, + is the center of mass, and the arrow indicates the positive (rightward) direction of the lateral displacement d_x.

Each condition was simulated once for 7 s. Both procedures begin with grasping and lifting the food. In drop release, opening begins with a minimum food–floor clearance of approximately 20 mm, measured from the lowest boundary vertex after subtracting R. In grounded release, the food is lowered until hard floor contact is detected. The fingers then remain closed for 10 ms before opening. The simulated finger gap increases at 34 mm/s, using the nominal experimental setting.

Table 1 Main settings of the model and operation

Category	Item	Value
Deformation	Young's modulus E, Poisson's ratio ν, SLS relaxation time, relaxation-branch fraction, yield strain	500 kPa, 0.49, 0.05 s, 0.5, 0.03

Category	Item	Value
Adhesion	Opening-work coefficient K_{G} ; rupture threshold G_{c} per bond (reference rupture opening δ_{b})	200 internal work units/ m^2 ; ON fingers and floor: 2×10^{-5} internal work units (0.447 mm); HIGH fingers: 1×10^{-4} (1.000 mm)
Adhesion	Normal/tangential compliances; adhesive-layer thickness t_{s}; local opening threshold ε	1×10^{-4} / 1×10^{-4} s^2 per model mass unit; 1 mm; $0.05R$
Contact	Contact radius R ; finger and floor static/kinetic friction; restitution	0.5 mm; 0.9/0.6; 0
Time integration	$\Delta t_{\mathrm{frame}}$; substeps; main solver iterations; duration; area-barrier lower-bound ratio; global velocity multiplier	$\frac{1}{120}$ s; 30; 1; 7.0 s; 0.03; 0.985 per frame (30th root per substep)
Operation	Lift/lower speed; opening speed; held finger-segment spacing; opening travel and duration	40 mm/s ; 34 mm/s gap speed (17 mm/s per finger); 22 mm ; 30.25 mm per finger in 1.779 s
Floor adhesion	Bond law and constants, activation (drop/grounded), hold time after grounding	Same constants as ON fingers; enabled at the start of opening, before finger motion; 10 ms hold after hard floor contact

Category	Item	Value
Evaluation	Hard floor-contact criterion; recording intervals	Clearance $\leq 10^{-9}$ m; frames every $\frac{1}{120}$ s; inversion and bond records every $\frac{1}{3600}$ s
Mesh and mass	Vertices; triangles; median initial edge length; lumped model mass	202 vertices (80 boundary); 322 triangles; approximately 1.3 mm; total mass 0.08 in simulator mass units, distributed by triangle area
Internal damping	Internal-edge damping time constant; triangle deformation and area-rate damping fractions	0.5 ms for normal and tangential edge motion; per-frame mixing fractions 0.3 and 0.7, respectively

Adhesion constants are uncalibrated internal settings.

The lateral displacement of the food center of mass is $d_{\mathrm{x}}(t) = x_{\mathrm{G}}(t) - x_{\mathrm{G}}(t_{\mathrm{open}})$, where t_{open} is the onset of gripper opening. Rightward displacement is positive. We record $d_{\mathrm{x}}(t)$, bond counts, detachment events, and first hard floor contact. In the simulations, a finger is considered attached while at least one of its bonds remains. The opening motion ends when the fingers stop. Snapshots use saved frame states; curves and event times use the substep records.

4.2 Drop-Release Behavior and Lateral Drag

Figure 4 shows the release motions obtained in the simulations. For S+·ON and S-·ON, the finger on the curved side lost its bonds first. The food remained attached to the finger on the flat-face side and moved with it. It subsequently moved downward and formed bonds with the floor. S0·ON also exhibited one-

sided motion, although the two fingers had equal bond counts at opening. The initial arrangement of interior mesh nodes was not symmetric about the vertical centerline. This asymmetry may have contributed to the food being dragged toward one finger, although its effect has not been isolated.

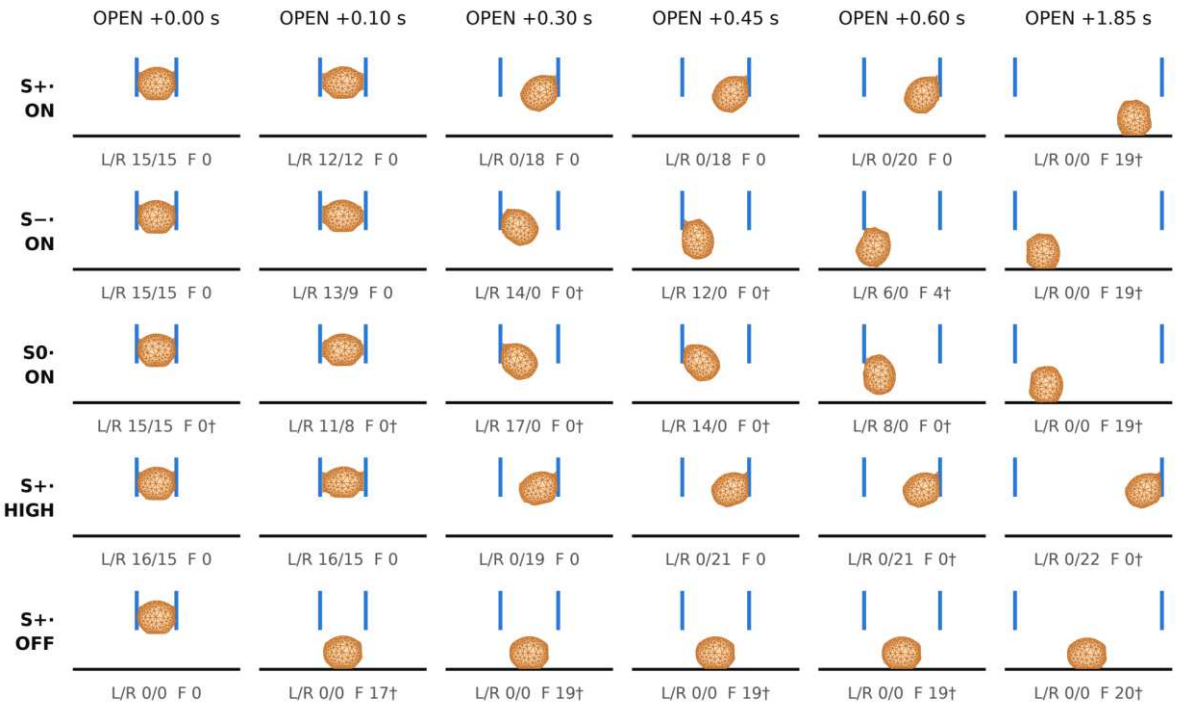

Fig. 4 Snapshots of drop release (from top: S+·ON, S−·ON, S0·ON, S+·HIGH, S+·OFF). Black lines: floor; blue lines: fingers; numbers: left/right finger bonds and floor bonds. A dagger marks snapshots after the first element inversion.

In S+·HIGH, the food remained attached to the right finger and stayed above the floor until the calculation ended. This retention continued after the first element inversion, 0.474 s after opening, and therefore describes the subsequent model behavior. In the OFF conditions, the food fell with little lateral motion after finger adhesion was disabled at opening. Section 4.3 relates these motions to the changes in bond counts.

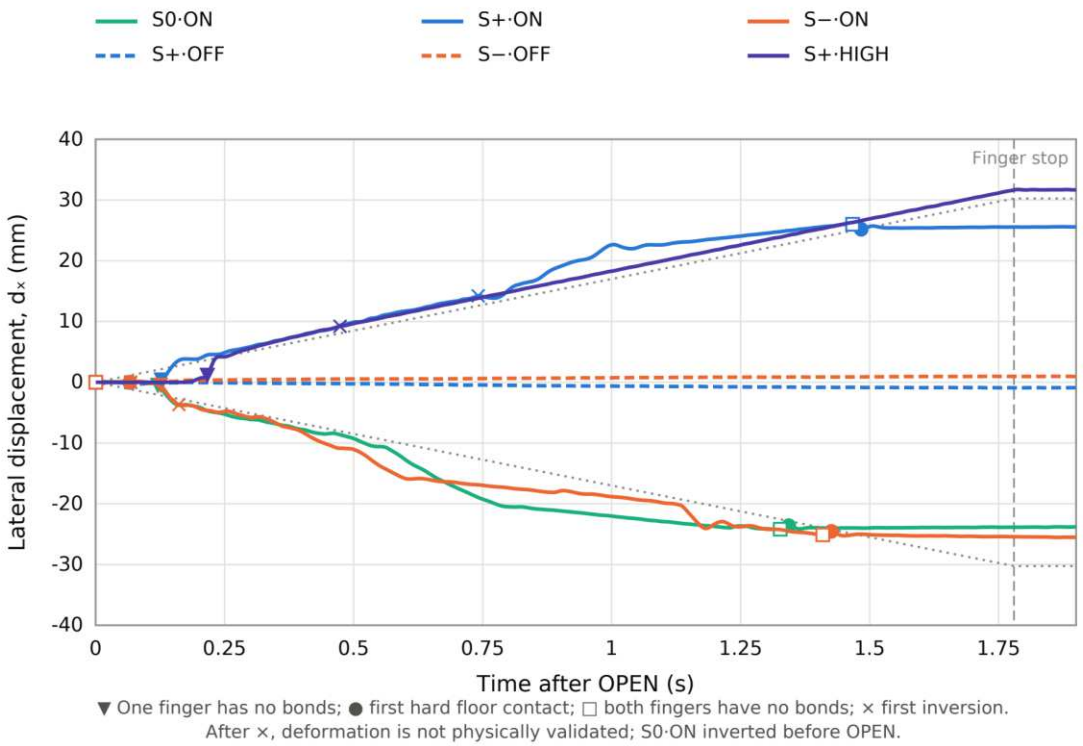

Fig. 5 Lateral displacement $d_x(t)$ for the six drop-release conditions. ▼: one finger loses all bonds; □: both fingers lose all bonds; ●: first hard floor contact; gray dotted curves: finger travel; dashed vertical line: finger stop; ×: first element inversion. S0·ON inverted before opening.

4.3 Bond Retention and Lateral Motion

The bond histories in Fig. 6 identify the finger associated with lateral drag. In S+·ON and S-·ON, both fingers had 15 bonds at opening. The curved-side finger lost all its bonds about 0.13 s later, while bonds remained on the flat-face side. The food then moved rightward for S+ and leftward for S- (Fig. 5). Equal bond counts do not imply equal bond openings: curved and flat contact geometries can develop different local separations under the same finger motion. This is a possible explanation for the different rupture times, but the responsible opening pattern has not been isolated.

New bonds also formed during release. In S+·ON, the right-finger count rose from 12 to 20. Bond records confirm formation during renewed contact, including at vertices that had previously lost a bond. Each event creates a new bond with zero history rather than restoring a broken bond.

As the S+·ON and S-·ON food moved downward, floor bonds appeared and the remaining finger bonds eventually disappeared. Both fingers were free of bonds about $1.4 - 1.5$ s after opening, before the fingers stopped.

In S+·HIGH, the curved-side finger lost all its bonds about 0.22 s after opening. The right finger retained 22 bonds at the 7 s calculation endpoint, beyond the interval displayed in Fig. 6, and no floor bonds formed. Together with the snapshots, this shows longer one-sided bond retention than in S+·ON under the limitations stated in Section 4.2.

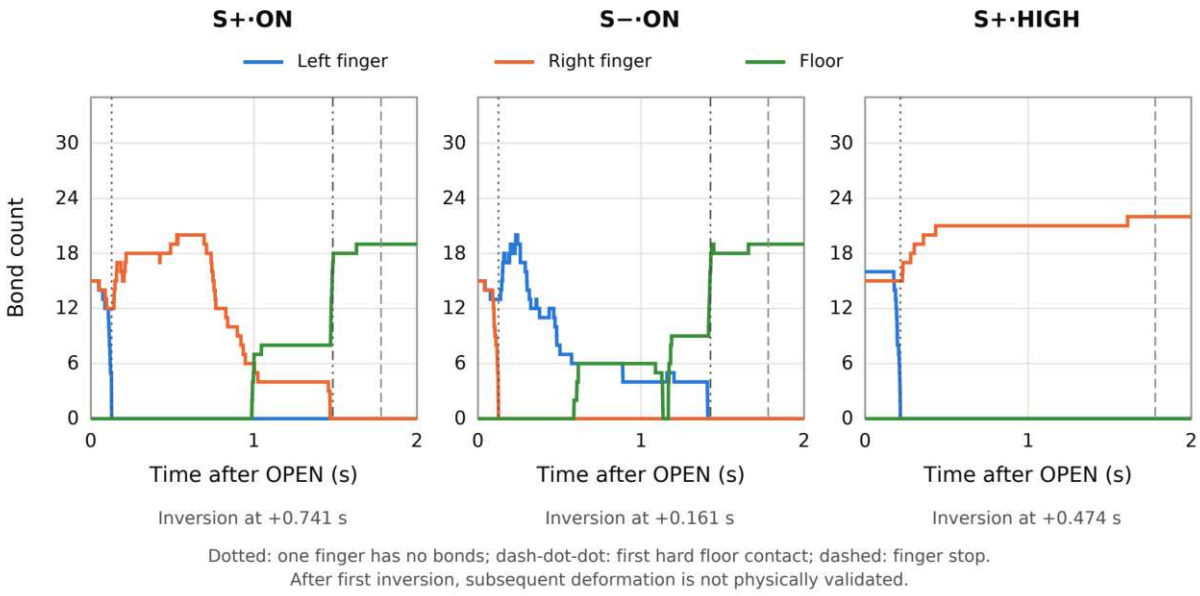

Fig. 6 Bonds remaining on the left finger, right finger, and floor. Conditions: S+·ON (left), S-·ON (middle), and S+·HIGH (right). Dotted vertical line: one finger loses all bonds; dash-dot-dot vertical line: first hard floor contact; dashed vertical line: finger stop. The displayed interval ends 2 s after opening; the text also reports the later calculation endpoint.

4.4 Grounded Release

Figure 7 shows snapshots of grounded release, and Fig. 8 shows the bond counts and lateral displacement. Floor adhesion was enabled at the start of opening, and floor bonds formed at eligible contacts. The finger bonds later disappeared, with longer retention in HIGH than in ON. The recorded lateral displacement remained below 8 mm in both grounded calculations, and was smaller than in the corresponding drop-release calculations. The displacement peaked shortly before the last finger bonds disappeared. These peaks and subsequent motions occurred after element inversion, so this comparison describes model behavior and does not quantify a physical placement benefit.

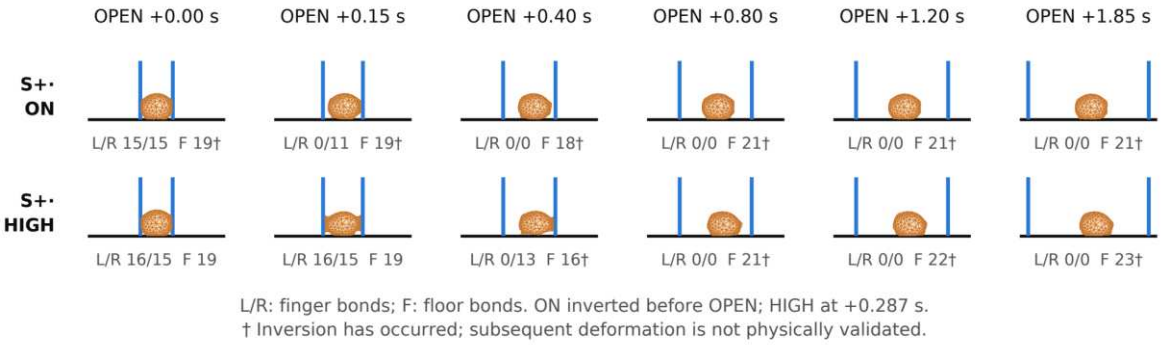

Fig. 7 Snapshots of grounded release (top: S+·ON; bottom: S+·HIGH). Numbers indicate left/right finger bonds and floor bonds. A dagger marks snapshots after the first element inversion.

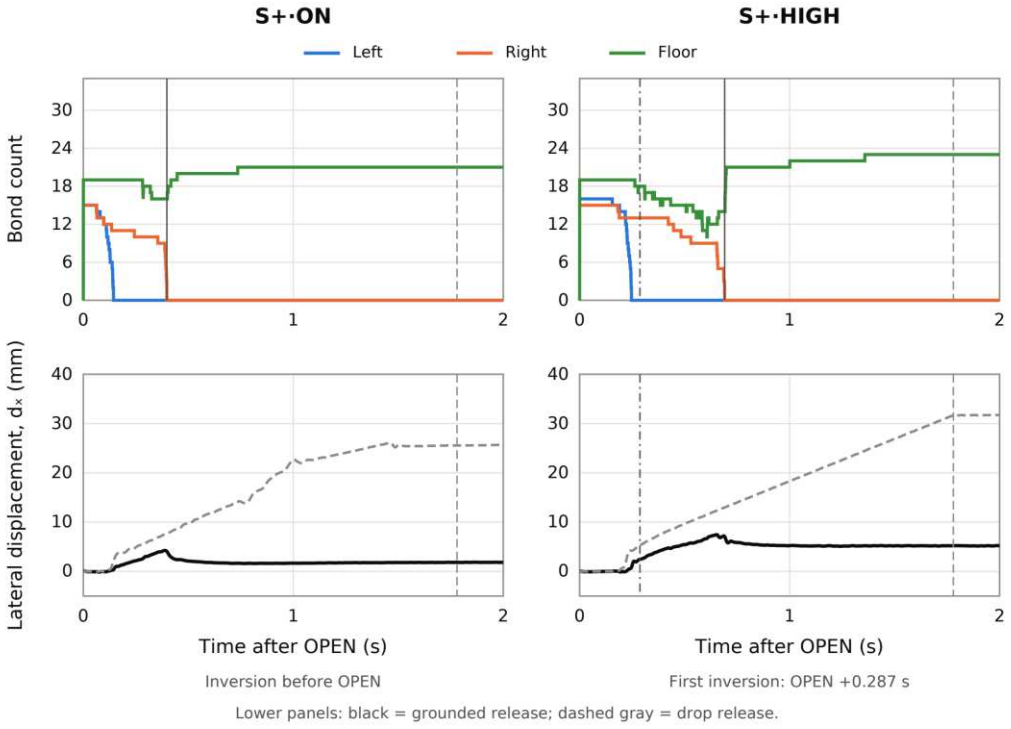

Fig. 8 Grounded-release bond counts (top) and lateral displacement $d_x(t)$ (bottom): S+·ON (left) and S+·HIGH (right). Thin solid vertical line: both fingers lose all bonds; dash-dotted vertical line: first element inversion; dashed vertical line: finger stop; gray dashed curve: drop release under the same adhesion condition. S+·ON inverted before opening.

5. Physical Release Experiments

5.1 Experimental Setup and Conditions

An electric gripper (IAI RCP2-GRST) was used, with stainless-steel plates attached to the finger pads as the contact surfaces (Fig. 9). The object was a commercially available Japanese rice cake (about 30 mm in diameter), and the placement surface was an acrylic board. Two release conditions were compared. Non-grounded release corresponds to drop release in the simulations: the food was lifted clear of the surface before the fingers opened. In grounded release, the food remained in contact with the surface. The finger gap during grasping was 14 mm.

The experimental records specify a nominal opening-speed setting of $34\ \mathrm{mm/s}$. In the seven evaluated non-grounded trials, however, the fingers stopped $1.03 - 1.20\ \mathrm{s}$ after the annotated opening onset, and the finger gap increased by approximately $56 - 61\ \mathrm{mm}$. The prescribed simulation motion, with a gap speed of $34\ \mathrm{mm/s}$ and an opening duration of $1.779\ \mathrm{s}$, therefore does not reproduce the measured experimental trajectory. The comparison below concerns motion patterns rather than matched trajectories. Seven non-grounded and four grounded trials had food-position annotations at both the opening and evaluation frames and were included in the displacement analysis. Two additional records lacked an opening-frame food annotation and were excluded.

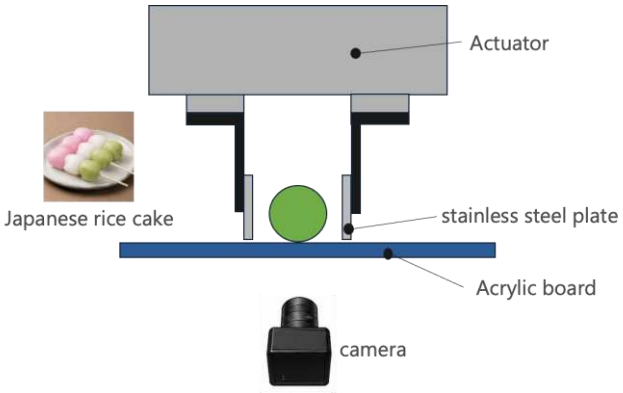

Fig. 9 Experimental setup.

5.2 Evaluation Metric

The measured food position is the area centroid of the segmented silhouette in each side-view image, used as a two-dimensional proxy for the center of mass. Silhouettes were extracted using GrabCut with manual foreground and background annotations. The final lateral displacement $d_{\mathrm{x,final}}$ is the change from the opening frame to the manually selected evaluation frame; the placement error is $|d_{\mathrm{x,final}}|$. These evaluation frames were labelled as settled in the annotations, but no numerical settling criterion was applied.

The videos were recorded at $119.88\,\mathrm{frames/s}$ with a resolution of 3840×2160 pixels. A known $14\,\mathrm{mm}$ distance gave scales of approximately $0.039 - 0.043\,\mathrm{mm/pixel}$. The uncertainty due to segmentation, calibration, and frame selection has not been quantified.

5.3 Experimental Results

The mean $|d_{\mathrm{x,final}}|$ was $22.24\,\mathrm{mm}$ in non-grounded release (7 trials) and $0.27\,\mathrm{mm}$ in grounded release (4 trials). The observed ranges did not overlap (Table 2).

In all seven non-grounded trials, one finger detached first, $0.13 - 0.39\,\mathrm{s}$ after opening, and the food moved with the other finger while still adhered to it. Three subsequent patterns were observed (Fig. 10(a), (b)). In the no-fall pattern (two trials), the food remained adhered to one finger through the evaluation frame. In the fall-after-stop pattern (two trials), it fell after the finger plate stopped. In these four trials, $|d_{\mathrm{x,final}}|$ was $25.5 - 28.7\,\mathrm{mm}$, close to the finger-plate travel of approximately $28 - 31\,\mathrm{mm}$.

In the fall-during-motion pattern (three trials), the food fell before the finger plate stopped. The complete-detachment time and the magnitude of final displacement were $(0.91\,\mathrm{s}, 23.1\,\mathrm{mm})$, $(0.47\,\mathrm{s}, 15.4\,\mathrm{mm})$, and $(0.63\,\mathrm{s}, 11.0\,\mathrm{mm})$. These three trials did not show a monotonic relation between detachment time and final displacement. Their displacements were smaller than those in the other two non-grounded patterns.

In grounded release, the measured lateral displacement remained small (Fig. 10(c)).

Table 2 Final lateral displacement by support condition

Condition	Evaluated trials	Mean $\lvert d_{\mathrm{x,final}}\rvert$ [mm]	SD [mm]	Range [mm]
Non-grounded	7	22.24	6.51	$11.02 - 28.71$
Grounded	4	0.27	0.16	$0.14 - 0.50$

(nominal opening-speed setting: $34\,\mathrm{mm/s}$). SD: standard deviation.

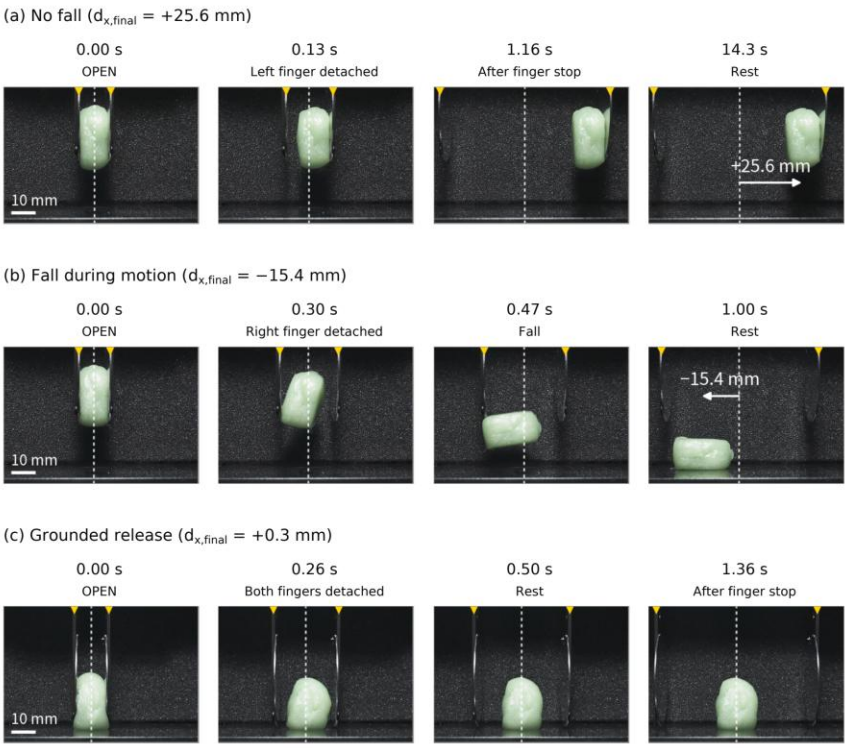

Fig. 10 Representative frames of the release experiments. (a) No fall: the food remained adhered to one finger through the evaluation frame; (b) fall during motion: the food fell before the finger stopped; (c) grounded release. Dotted line: tracked food position at opening; ▼: finger plate; arrow: $d_{x,final}$. Times are measured from the start of opening. "Rest" denotes the manually selected evaluation frame.

6. Qualitative Comparison with Experiments and Discussion

6.1 Qualitative Comparison

Table 3 compares the experimental and simulated motions. In both the experiments and simulations, the food moved laterally while attached to one finger. In some experiments, attachment lasted until or after finger stopping. In the S+·HIGH simulation, finger bonds remained at the simulation endpoint. Grounded release produced little lateral motion in the experiments and less displacement than drop release in the

simulations. The simulated grounded results include motion after element inversion. Different experimental and simulated finger trajectories and uncalibrated model parameters prevent quantitative comparison of detachment timing and final placement.

Table 3 Qualitative comparison of release behavior.

Behavior	Physical experiments	Simulations
Residual adhesion	One finger detached first in all non-grounded trials.	One-sided bonds remained in the ON and HIGH drop-release cases.
Lateral drag	The food moved with the finger to which it remained attached.	The food moved toward the side with remaining finger bonds.
Continued attachment	In some trials, the food remained attached until or beyond finger stopping.	S+·HIGH retained finger bonds to the endpoint, after inversion.
Grounded release	Final lateral displacement was $0.14 - 0.50$ mm.	Recorded peaks were about 4 mm (ON) and 7 mm (HIGH), smaller than in drop release; both occurred after inversion.

Simulation entries describe the model behavior under the limitations stated at the start of Section 4.

6.2 Discussion and Future Work

In the non-grounded experiments, the food moved laterally with the finger to which it remained attached. The experimental no-fall and fall-after-stop trials had final displacements close to the finger-plate travel. The three experimental trials with detachment during finger motion had smaller final displacements,

although earlier detachment did not always give a smaller displacement (Section 5.3). The experimental results therefore link lateral displacement to finger travel while attachment persists. In the ON simulations, the food followed the finger with remaining bonds after the other finger lost all its bonds. The experiments and simulations thus showed similar one-sided following.

In the present adhesion model, damage increases only when effective opening exceeds its previous maximum. The model does not represent damage that develops over time at fixed opening. Future work should introduce a time-dependent damage law and validate it against experiments under sustained loading.

In the grounded experiments, all four trials had a final lateral displacement of 0.5 mm or less. In the grounded S+·ON simulation, the recorded lateral displacement was smaller than in the S+·ON drop-release simulation. In the grounded S+·HIGH simulation, raising only the finger-bond rupture threshold prolonged attachment and increased lateral drag along the floor relative to grounded S+·ON. These simulation results suggest that release depends on the balance between floor restraint and finger attachment. However, the simulations used the ON finger-bond law and constants for the floor, including in HIGH (Table 1). In the experiments, the relative strengths of finger–food and floor–food adhesion were not measured. The experimental grounded condition therefore cannot yet be directly equated with S+·ON. Testing this interpretation requires separate adhesion measurements at the two physical interfaces and simulation comparisons that isolate support, friction, and adhesion.

The simulation study has several limitations. The model is two-dimensional, and each condition was simulated once. The model parameters have not been calibrated against experimental data; adhesion work and rupture threshold are expressed on an internal model scale. The simulations used 30 substeps per frame, but time-step and mesh convergence have not been assessed. Element inversion occurred in every simulated condition, and its effect on subsequent simulated motion remains unknown. Future simulations should prevent inversion and assess convergence with smaller time steps and finer meshes. Future experiments should measure material properties and force–displacement responses at the finger–food and floor–food interfaces to identify model parameters and compare adhesion strengths. Repeated experiments

and simulations with varied initial conditions, together with a three-dimensional model, are needed to assess variability and reproducibility. For quantitative comparisons between the simulations and experiments, the simulations should use the finger trajectories measured in the experiments.

7. Conclusions

This study developed a two-dimensional model as a step toward a simulation environment for learning robotic food-release strategies. The model combines XPBD deformation with adhesive bonds that track maximum effective opening and internal opening work. Damage governs rupture, while normal and tangential compliances remain fixed until bond removal.

In the drop-release simulations, the food followed the finger with remaining bonds when finger adhesion was retained. For S+ and S-, this was the finger on the flat-face side. Disabling finger adhesion produced a fall with little lateral motion. In the grounded-release simulations, lateral displacement was smaller than in drop release. Increasing the finger-bond rupture threshold prolonged attachment and increased lateral drag along the floor.

The experiments and simulations showed qualitative similarities in one-sided following and reduced lateral displacement with grounded release. These observations support further development of the model, but element inversion, uncalibrated parameters, and differences in finger motion currently limit physical interpretation and quantitative prediction.

List of abbreviations

XPBD, Extended Position-Based Dynamics; PBD, Position-Based Dynamics; IPC, Incremental Potential Contact; SLS, standard linear solid; SD, standard deviation.

Declarations

Availability of data and materials

The datasets used and/or analysed during the current study are available from the corresponding author on reasonable request.

Competing interests

The authors declare that they have no conflict of interest.

Funding

This work was partly supported by KAKENHI 23H00492.

Authors' contributions

R.A. drafted the manuscript. K.Y. supervised the study and reviewed and edited the manuscript. J.T. reviewed the manuscript.

Acknowledgements

This work was partly supported by KAKENHI 23H00492.

References

[1] Wang Z, Hirai S, Kawamura S (2022) Challenges and Opportunities in Robotic Food Handling: A Review. Front. Robot. AI 8:789107.

[2] Qiu Z, Paul H, Wang Z, Hirai S, Kawamura S (2023) An Evaluation System of Robotic End-Effectors for Food Handling. Foods 12(22):4062.

[3] Ueda D, Kurihara D, Aruga T, Endo G (2026) Experimental Verification of Vibration-Based Release for a Sticky-Food Handling Gripper. In: Proc. IEEE/SICE Int. Symp. Syst. Integr. (SII).

[4] Müller M, Heidelberger B, Hennix M, Ratcliff J (2007) Position Based Dynamics. J. Vis. Commun. Image Represent. 18(2):109–118.

[5] Bender J, Koschier D, Charrier P, Weber D (2014) Position-Based Simulation of Continuous Materials. Comput. Graph. 44:1–10.

[6] Macklin M, Müller M, Chentanez N (2016) XPBD: Position-Based Simulation of Compliant Constrained Dynamics. In: Proc. Int. Conf. Motion in Games (MIG), pp 49–54.

[7] Gascón J, Zurdo JS, Otaduy MA (2010) Constraint-Based Simulation of Adhesive Contact. In: Proc. Eurographics/ACM SIGGRAPH Symp. Comput. Anim. (SCA), pp 39–44.

[8] Fang Y, Li M, Cao Y, Li X, Wolper J, Yang Y, Jiang C (2024) Augmented Incremental Potential Contact for Sticky Interactions. IEEE Trans. Vis. Comput. Graph. 30(8):5596–5608.

[9] Suzuki K, Mizuuchi I (2024) Simulating Adhesion between Food Ingredients and Separating Them Using Reinforcement Learning. In: Proc. JSME Conf. Robot. Mechatron., Article 2P2-G01. https://doi.org/10.1299/jsmermd.2024.2P2-G01.

[10] Liang X, Zhang Y, Liu F, Richter F, Yip MC (2025) AutoPeel: Adhesion-Aware Safe Peeling Trajectory Optimization for Robotic Wound Care. In: Proc. IEEE Int. Conf. Robot. Autom. (ICRA), pp 6153–6160.

[11] Macklin M, Storey K, Lu M, Terdiman P, Chentanez N, Jeschke S, Müller M (2019) Small Steps in Physics Simulation. In: Proc. ACM SIGGRAPH/Eurographics Symp. Comput. Anim. (SCA), Article 39, pp 1–7.

[12] Sifakis E, Barbič J (2012) FEM Simulation of 3D Deformable Solids: A Practitioner's Guide to Theory, Discretization and Model Reduction. In: ACM SIGGRAPH 2012 Courses, Article 20, pp 1–50.